Journal of Strain Analysis for Engineering Design
XX(X):2–17

DOI: 10.1177/ToBeAssigned
www.sagepub.com/
SAGE

Effect of different helmet shell configurations on the protection against head trauma

Marta Palomar[1], Ricardo Belda[1] and Eugenio Giner[1]

Abstract

Head trauma following a ballistic impact in a helmeted head is assessed in this work by means of finite element (FE) models. Both the helmet and the head models employed were validated against experimental high rate impact tests in a previous work. Four different composite ply configurations were tested on the helmet shell and the energy absorption and the injury outcome resulting from a high-speed impact with full metal jacket bullets were computed. Results reveal that hybrid aramid-polyethylene configurations do not prevent from bullet penetration at high velocities, while 16-layer aramid configurations are superior in dissipating the energy absorbed from the impact. The fabric orientation of these laminates proved to be determinant for the injury outcome, as maintaining the same orientations for all the layers led to basilar skull fractures (dangerous) while alternating orientation of the adyacent plies resulted in an undamaged skull. To the authors knowledge, no previous work in the literature has analysed numerically the influence of different stack configurations on a single combat helmet composite shell on human head trauma.

Keywords

Combat helmet design, ballistic protections, blunt trauma, protective materials.

Prepared using sagej.cls *[Version: 2017/01/17 v1.20]*

Introduction

Ballistic head injuries have increasing relevance in the current context of military conflicts and terrorism activities[1]. Worldwide market for personal protection systems is worth between 300 and 400 million euros per year and it is increasing at a 5% rate each year[2]. Over the last decades, many attempts have been made to improve the effectiveness of combat helmets, where tendencies are to substitute heavy metallic helmets by composite shells, which have appeared with great potential to develope ligthweight personal protections. Helmet failure following ballistic impacts on laminated composites gives rise to new personal injuries compared to the metallic ones, as the increased penetration resistance is related to larger surface deformations. This non-penetraating injury is called Behind Helmet Blunt Trauma (BHBT) and results from the strike of the inner surface of the helmet to the head[3,4]. This damage mode is quantified through the so-called Back Face Deformation (BFD) measurement[5], which needs to be accounted in the standards for helmet designs.

Some works in the literature address the study of the effect of different shell configurations experimentally[2,6,7] to assess BHBT on helmeted heads, headforms or surrogates[8–11]. In Salman et al.[2], an experimental evaluation of ballistic impact tests against woven kenaf/aramid-reinforced polyvinyl butyral hybrid composite helmets was performed, aiming to identify the best architecture laminate configuration fulfilling the U.S. military PASGT requirements. The damage mechanisms of each configuration were examined visually after testing, analyzing cross-sections of the samples. Sarron et al.[8] carried out ballistic impact experiments using human cadaver heads and skulls and highlighted the strong influence of the protective properties and the distance to the skull on skull fracture and brain injury.

Ultra-high molecular weight polyethylene (UHMWPE) fiber-based composites are employed in personal protection systems due to their specific strength and elastic wave speed[11], but its great energy absorption produces high deformations which may be dangerous even with no bullet penetration. The impact stresses during non-penetrating ballistic impacts were analyzed in Vargas and Gurganus[11]. They assessed the BHBT using a ballistic gelatin as brain surrogate and applied digital image correlation to examine full-field deformations during testing.

[1]Centre of Research in Mechanical Engineering - CIIM, Dept. of Mechanical Engineering and Materials, Universitat Politècnica de València, Camino de Vera, 46022 Valencia, Spain

Corresponding author:
Marta Palomar
Email: marpato@etsid.upv.es

Prepared using sagej.cls

Ballistic impact investigations through experimental studies involve high costs and are time-consuming, whereas numerical models permit to simulate different configurations reducing costs. Numerous investigations on the numerical modeling of damage in composites under ballistic impacts are available in the literature[6,7,12–16]. In a recent work, Bandaru et al.[6] proposed a constitutive model to study damage initiation and propagation on composite laminates under ballistic impacts based on continuum damage mechanics. Their model includes cohesive elements between layers in order to account for delamination failure. Yang and Chen[16] investigated through finite element modeling the energy absorption efficiency of layer configurations proposing some guidelines for hybrid design of ballistic armour panels. Other authors, like Martínez et al.[7] modeled impact tests of a steel sphere against a hybrid laminate composed by nonwoven and woven fabrics using numerical simulations that accounted for a mesoscale description of the woven fabrics and a multiscale approach for the nonwoven fabrics. They highlighted the energy dissipation capability of the nonwoven fabric compared to the woven shield.

The purpose of this work is to study different shell configurations in order to assess the feasibility of incorporating hybrid compositions for the design of personal head protections. This improves the feasibility of reducing actual helmets weight without compromising their protective efectiveness. Specifically, four different composite stack configurations distinguishing between aramid and hybrid will be investigated. The protective effectiveness is investigated through the analysis of a finite element model of a helmeted human head where each stack configuration is simulated. This work is structured as follows: first, a section describing the methodology used to develop the numerical baseline model for the ballistic simulations. Then the different helmet shell configurations are simulated. After that, a Results section presents the most relevant outcome obtained from each numerical test, which are commented in the Discussion section. Finally, the most significant conclusions of the work will be pointed out.

Materials and methods

Head model

A human head numerical model developed from the segmentation of computed tomography (CT) images from a man belonging to the 50% percentile was employed in this work. This model was validated in previous works by the authors[17] against low to middle velocity impact tests from the literature[18,19] and against ballistic experimental tests[20] on protected postmortem human surrogate (PMHS) heads[8]. The

model comprises six of the main living tissues of the head: cranium (divided into the two compact bone tables and the diplöe core), facial bones, brain, cerebrospinal fluid (CSF) and scalp. The result is a mesh of 379000 tetrahedral elements (C3D4 in Abaqus[21]). The model with its different layers is depicted in Fig. 1.

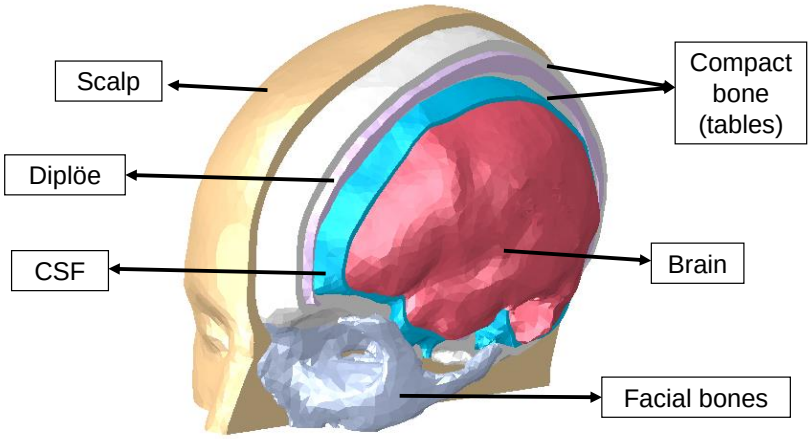

Figure 1. Numerical head model from[17,20] employed for ballistic simulations.

All the head tissues except for the brain tissue were modelled as linear elastic materials (Table 1), as assumed in other works from the literature. Brain tissue was considered an hyperelastic material defined by the Mooney-Rivlin law, where the strain energy potential is defined as follows:

$$W = C_{01}(\overline{I}_2 - 3) + C_{10}(\overline{I}_1 - 3) + D_1(J-1)^2 \tag{1}$$

$$D_1 = \frac{2}{K}$$

being W the strain energy potential, $\overline{I}_1$ and $\overline{I}_2$ the linear and quadratic invariants of the Cauchy-Green tensor, J the determinant of the deformation gradient and K the bulk modulus of the material. For almost non-compressible materials, $J \approx 1$. As the brain is a nearly incompressible tissue due to its high water content, special care was taken to avoid unstabilities and noise during the calculation. Therefore, double precision was required both for the preprocessor and for the processor[21].

Additionally, its viscoelastic behaviour was added as a time-dependent Prony series defined by

$$G(t) = G_0 - \sum_{i=1}^{N} G_i \left(1 - e^{(-t/\tau_i)}\right) \tag{2}$$

where G_0 is the initial shear modulus, and G_i, τ_i define points of the curve from stress-relaxation tests. Brain tissue hyper-viscoelastic properties were implemented in Abaqus Explicit using the values defined in Table 2.

In order to simulate certain outcomes like skin laceration and skull fracture, a user subroutine (type VUSDFLD[22]) has been implemented for the scalp layer and the cranial tissues. This subroutine, which accesses the maximum principal stress and strain values at each element for each iteration, allows to delete those elements whose values exceed a certain threshold value for failure. For the scalp tissue, this threshold is set in terms of strain, with an ultimate value of 0.7. The bony tissues failure is characterised by means of Rankine's criterion setting the values of $\sigma_{\text{u,t}} = 90$ MPa and $\sigma_{\text{u,c}} = -132$ MPa for compact bone and $\sigma_{\text{u,t}} = 34.8$ MPa, $\sigma_{\text{u,c}} = -24.8$ MPa for the diploë layer[23]. It is important to highlight that the skull fracture response against ballistic impact of this numerical model has been previously validated against Sarron et al.[8] experiments. Therefore, the head model is suitable for capturing the different fracture patterns, which is a key point in the present work.

	Tables	Diplöe	Face	Scalp	CSF
$\rho(\text{kgm}^{-3})$	1800	1500	3000	1130	1000
$E(\text{MPa})$	15000	4500	15000	16.7	1.26
ν	0.21	0.22	0.21	0.42	0.4999
$\sigma_{\text{u,c}}(\text{MPa})$	-132	-24.8	-	-	-
$\sigma_{\text{u,t}}(\text{MPa})$	90	34.8	-	-	-

Table 1. Material properties of the head tissues (from Palomar et al.[20]).

Properties	Hyperelastic constants	Viscoelastic constants
ρ = 1040(kgm^{-3})	C_{01}=62 Pa	g_1=0.636, g_2=0.363
K= 0.21 GPa	C_{10}=69 Pa	τ_1=0.008, τ_2=0.15

Table 2. Hyper-viscoelastic properties of brain tissue.

Helmet model

A combat helmet with the geometry of an Advanced Combat Helmet (ACH) was modelled and meshed employing linear hexaedra (type C3D8 in Abaqus), with a mesh refinement in the frontal area where the ballistic impact will take place. The baseline helmet geometry comprised four different composite stack configurations, distinguishing between aramid and hybrid (detailed in Fig. 2).

Table 3. Different helmet shell configurations tested in this work.

Config.	Description	Shell thickness [mm]	Shell mass [kg]
#S1	16 aramid-fabric plies (thickness 0.5 mm each), all with the same orientation	8	1.03
#S2	16 aramid-fabric plies (thickness 0.5 mm each), with alternating orientations of 0°/90°and 45°/-45°between adjacent plies	8	1.03
#S3	hybrid configuration of 4 plies of aramid fabric (thickness 0.4 mm each) in the striking surface and 24 of UHMWPE	7.36	0.79
#S4	hybrid configuration of 8 plies of aramid fabric (thickness 0.4 mm each) in the striking surface and 24 of UHMWPE	8.96	1.01

Material properties for the aramid woven layers have been obtained from Tan et al.[24]. The mechanical behaviour of aramid against high speed impact was complemented with a VUMAT subroutine including a modified version of the Hashin's damage criterion for fabrics. This subroutine was validated against ballistic impact against 9 mm FMJ ammunition at impact velocities of 425 $\pm$ 15 ms^{-1} in Rodríguez-Millán et al. (2016)[26]. The failure modes considered are summarised in Table 4, where the first four apply for intralaminar (fiber) failure while the last two account for interlaminar (matrix) failure. X_{it}, X_{ic} denote tensile and compressive strength in the i direction, while S_{ij} are referred to shear strengths.

The UHMWPE material has been modelled as described by Lässig et al.[27] and Nguyen et al.[28]. The material employed by Lässig et al. is Dyneema HB26, which consists of unidirectional plies reinforced with UHMWPE fibers at 0°which are alternatedly stacked with plies oriented at 90°by hot-pressing. Therefore, the material

can be treated as orthotropic[27], and the same assumption has been taken in the helmet model discussed in this work. The modelling strategy for the UHMWPE panels has been taken from Nguyen et al.[28] as it provides a good agreement between their ballistic tests and their numerical results at a velocity range which includes the impacts studied in this work. Thus, the material has been discretised in several layers (24) in order to achieve more accurate results both in terms of BFD and energy absorption.

The material behaviour of the polyethylene shell is modeled in Abaqus/Explicit using an orthotropic elasticity law in conjunction with an orthotropic plasticity model. Failure is assessed by means of a damage law. In Lässig et al.[27] this same material accounts additionally for an $U_s - U_p$ equation of state (EOS), but it has not been implemented in the model of this study as the impact velocities remain in the ballistic regime and do not achieve hypervelocity conditions. Therefore, the contribution of the equation of state would be negligible.[27] The material constants for the material description have been taken from Nguyen et al.[28]

Failure mode	Equation
Fiber tension ($\sigma_1 > 0$)	$\mathrm{d_{ft1}} = \left(\frac{\sigma_1}{\mathrm{X_{1t}}}\right)^2 + \left(\frac{\tau_{12}}{\mathrm{S_{12}}}\right)^2 + \left(\frac{\tau_{13}}{\mathrm{S_{13}}}\right)^2$
Fiber compression ($\sigma_1 < 0$)	$\mathrm{d_{fc1}} = \left(\frac{\sigma_1}{\mathrm{X_{1c}}}\right)^2 + \left(\frac{\tau_{12}}{\mathrm{S_{12}}}\right)^2 + \left(\frac{\tau_{13}}{\mathrm{S_{13}}}\right)^2$
Fiber tension ($\sigma_2 > 0$)	$\mathrm{d_{ft2}} = \left(\frac{\sigma_2}{\mathrm{X_{2t}}}\right)^2 + \left(\frac{\tau_{12}}{\mathrm{S_{12}}}\right)^2 + \left(\frac{\tau_{23}}{\mathrm{S_{23}}}\right)^2$
Fiber compression ($\sigma_2 < 0$)	$\mathrm{d_{fc2}} = \left(\frac{\sigma_2}{\mathrm{X_{2c}}}\right)^2 + \left(\frac{\tau_{12}}{\mathrm{S_{12}}}\right)^2 + \left(\frac{\tau_{23}}{\mathrm{S_{23}}}\right)^2$
Matrix tension ($\sigma_3 > 0$)	$\mathrm{d_{mt}} = \left(\frac{\sigma_3}{\mathrm{X_{3t}}}\right)^2 + \left(\frac{\tau_{13}}{\mathrm{S_{13}}}\right)^2 + \left(\frac{\tau_{23}}{\mathrm{S_{23}}}\right)^2$
Matrix compression ($\sigma_3 < 0$)	$\mathrm{d_{mc}} = \left(\frac{\sigma_3}{\mathrm{X_{3c}}}\right)^2 + \left(\frac{\tau_{13}}{\mathrm{S_{13}}}\right)^2 + \left(\frac{\tau_{23}}{\mathrm{S_{23}}}\right)^2$

Table 4. Failure criteria for fabrics implemented in the VUMAT subroutine

The interior of the helmet was completed with a seven pad cushioning system tied to the inner surface of the helmet shell. Each pad was modelled through the low density foam material option from Abaqus. To model this foam behaviour, stress-strain data from uniaxial tension and compression tests at different strain rates are

implemented. Finally, the Full Metal Jacket (FMJ) bullet is modelled following the geometry described for 9 mm Parabellum bullets in Tham et al.[29] . The model consists of two parts: a lead core and a brass jacket. The first part is modelled by means of an equation of state (EOS), while the second one is defined by a plasticity Johnson-Cook model with damage initiation. The mechanical parameters applied to the two components of the projectile have been extracted from Tse at al.[30]

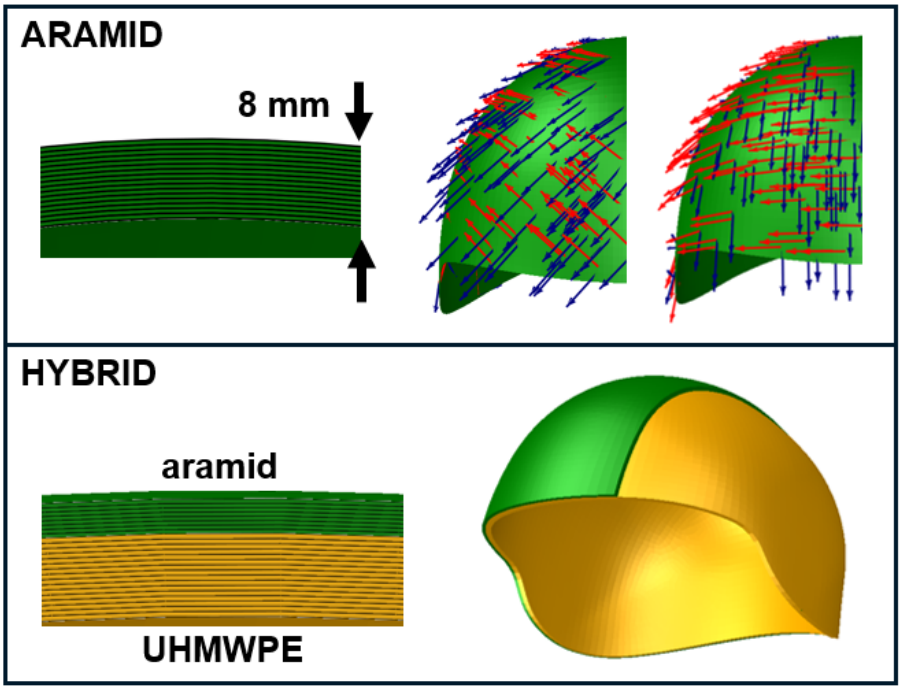

Figure 2. Configurations tested in this study. Aramid-only shell with 16 plies for #S1 and #S2 (top left). Top right: the two different aramid fabric orientations (45°/-45°and 0°/90°). Bottom: scheme of the hybrid configurations #S3 and #S4, where aramid layers are placed in the striking surface of the helmet (green) and UHMWPE in the inner shell (yellow).

Assembly and boundary conditions

The helmet model was inserted in the head through a pre-step in which the helmet moved vertically at a low speed until reaching the head and then it was held in the position in which there was no motion in the internal foam pads, thus ensuring a proper adjustment. The entire set-up for the ballistic simulations is depicted in Figure 3.

A free boundary condition was set to the head model due to the short duration of the impact event. Long term response of the head tissues will not be assessed in this

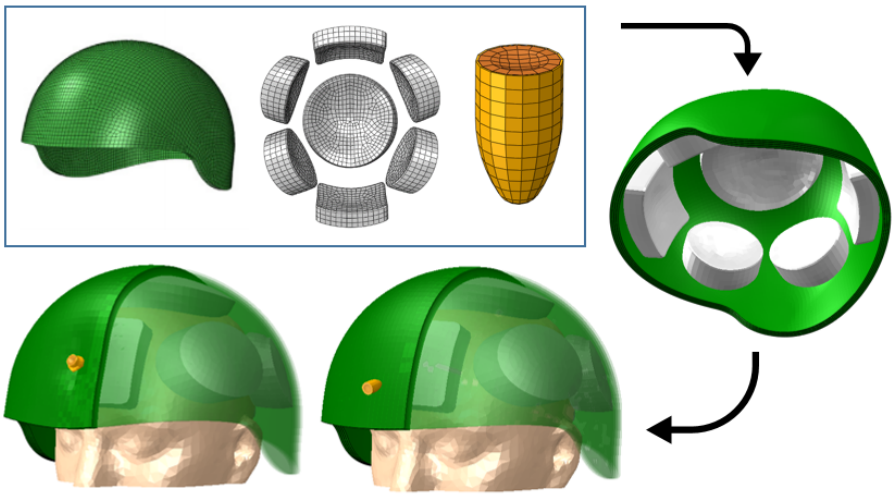

Figure 3. Coupling of the head and helmet models by means of Abaqus/Explicit. Complete helmet model with the foam padding sticked to the inner shell (right) and insertion in the head model ensuring contact with the foam pads (bottom).

work so the absence of a strapping system in the helmet model will not compromise the accuracy of the results. A prescribed velocity of 530 m/s is set to the bullet in a direction perpendicular to the helmet surface in its frontal region. The contact interaction between the bullet and the helmet is set as general contact[21] while the interaction between each of the helmet plies is defined by a cohesive behaviour, in order to allow for delamination phenomena. A friction coefficient of 0.18 was established between the FMJ bullet and the aramid fabric layer, as suggested in Wisniewski and Gmitrzuk[31].

Hourglass energy was controlled during the simulation, ensuring that the artificial strain energy (output variable employed in Abaqus[21] to characterise hourglass) remains lower than the 5% of the total energy.

Results

Four simulations, each with one of the helmet configurations #S1 to #S4 were performed. Von Mises stress distributions varying with time for each case are depicted in Fig. 4. In configurations #S3 and #S4, the last image of the sequence corresponds to the moment in which the bullet perforates the helmet. In the other two cases, the last image depicts the stress distribution in the instant where the helmet shell deformation reaches its maximum value.

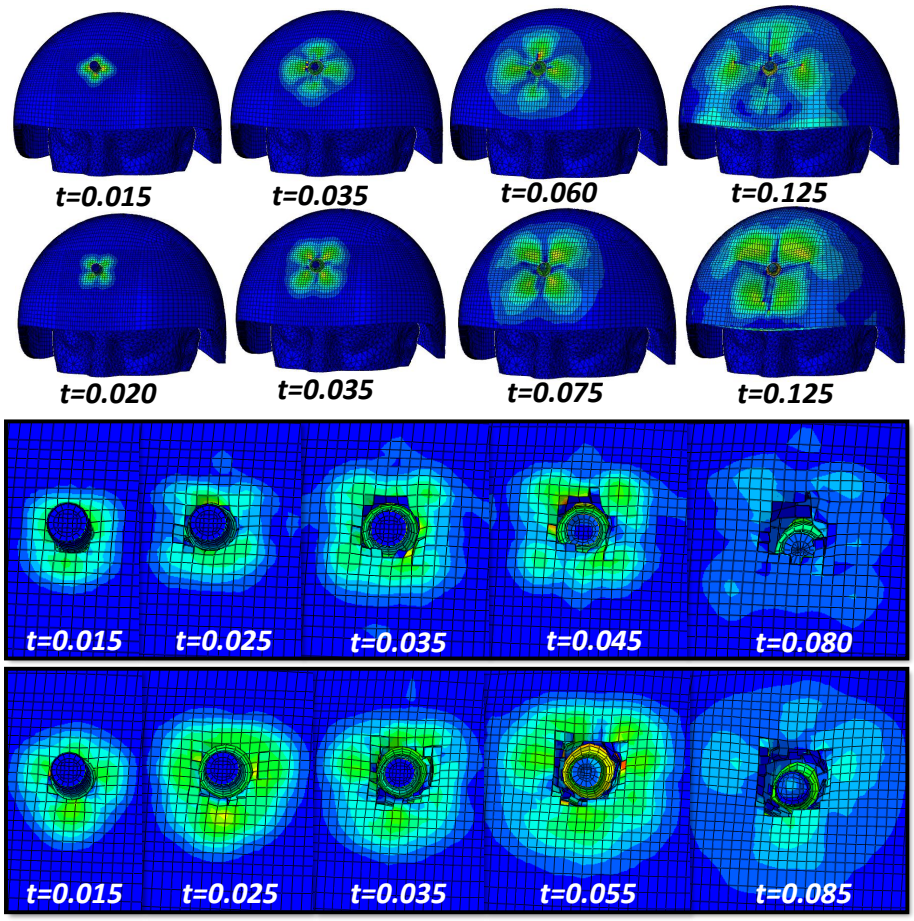

Figure 4. Von Mises stress distributions on the frontal helmet shell for the four configurations simulated: #S1 (top), #S2 (middle top), #S3 (middle bottom), #S4 (bottom). All the time values are expressed in ms.

The energy absorbed by the helmet shell was computed for all the simulations, and depicted in Fig. 5. It can be clearly observed that the aramid configurations absorb most of the impact energy (67 and 61% of the bullet kinetic energy for configurations #S1 and #S2 respectively). The hybrid configurations, on the contrary, have a considerably lower contribution to the energy dissipation (37 and 44% for #S3 and #S4, respectively) and the absorption stops once the bullet has perforated all the layers of the shell, then allowing the remaining impact energy to directly reach the head.

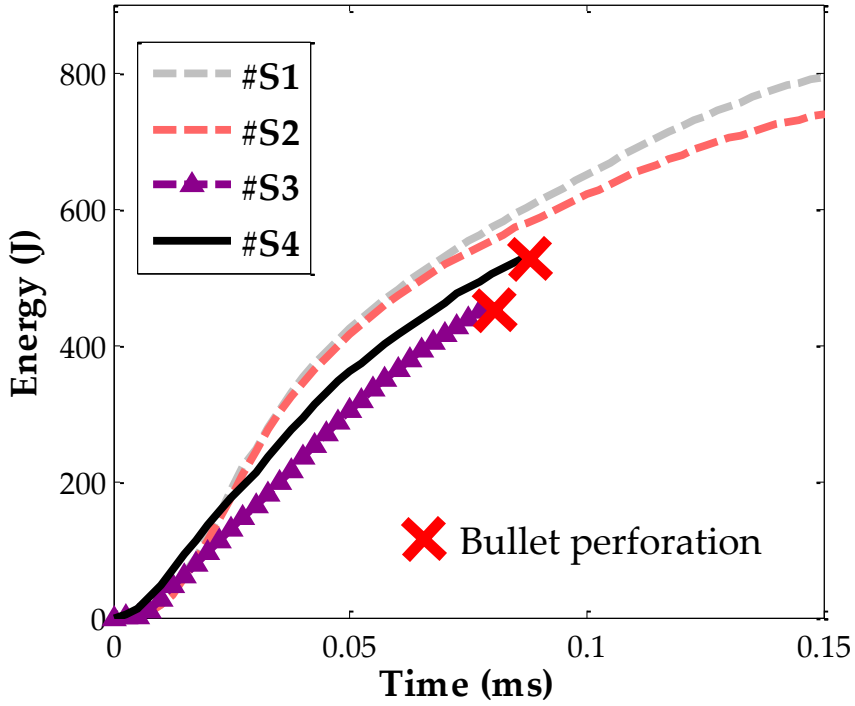

Figure 5. Impact energy absorbed by the helmet shell with each of the four configurations tested.

By means of the VUSDFLD subroutine implemented for the skull bones, the failed elements after each simulation were identified and depicted, to reveal the corresponding skull fracture patterns shown in Fig. 6.

Discussion

Frontal ballistic impact simulations on a head protected with an ACH with four different shell configurations have been performed in this work, using FMJ bullets as ammunition with an initial speed of 530 m/s. Our results reveal a strong dependency of the impact energy absorption capacity of the helmet on its stack configuration. In this work, two of the shells tested comprised only aramid layers (#S1,#S2), and both were able to prevent the penetration of the bullet, as shown in Fig 5. The impact energy dissipated in fiber breaking and delamination of the plies was sufficient to fully

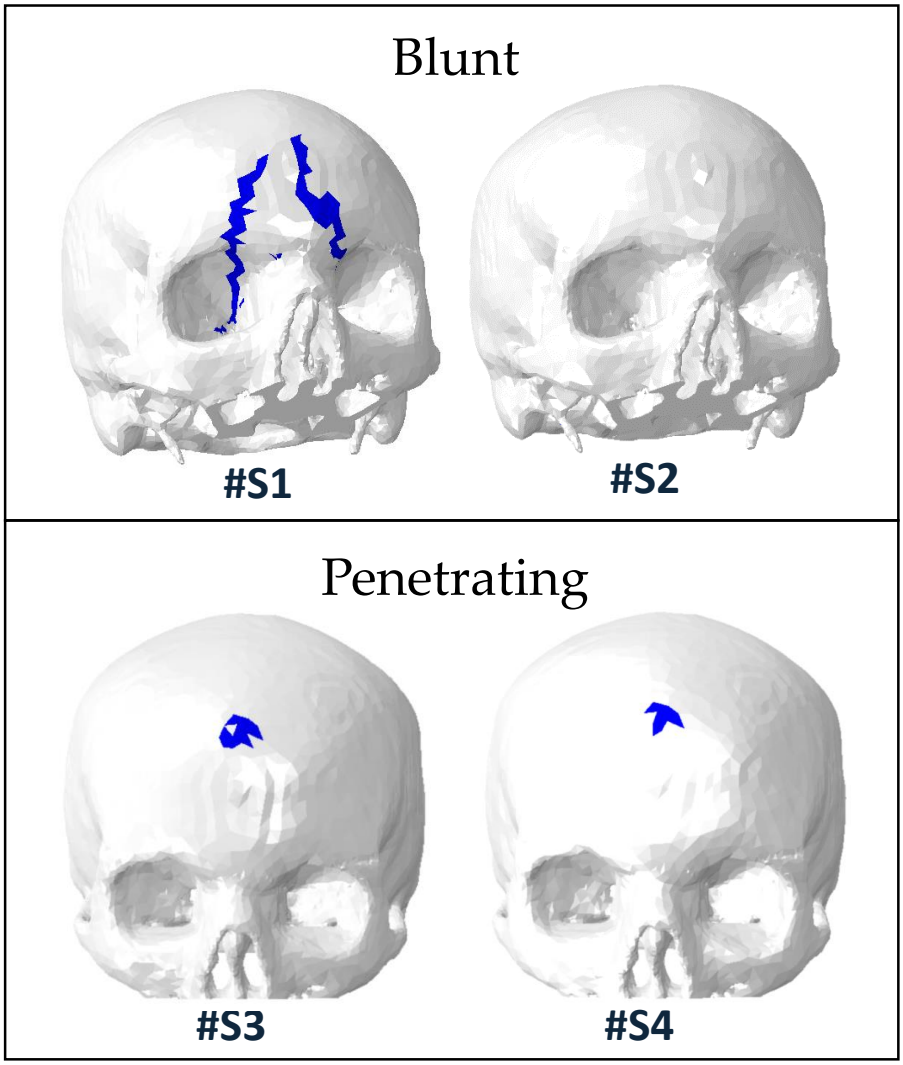

Figure 6. Skull fracture patterns obtained after each simulation. Case #S1: basilar skull fracture, case #S2: no visible fractures, cases #S3 and #S4: penetration of the bullet.

attenuate the movement of the bullet. This was not the case for hybrid configurations #S3 and #S4, where the penetration of the bullet occurs around 0.08 ms after the impact. Configuration #S4, which comprised four more aramid layers on its striking surface than #S3, is able to absorb a 7% more of the total energy with respect to the latter. Bullet penetration is also delayed by the addition of aramid layers on the striking surface. Despite the fact that the helmet shell thickness in configuration #S4 is almost

1 mm greater than the only-aramid ones, there is no corresponding increment either in energy absorption or prevention of penetration. These results are in agreement with the reported by Rafaels et al. (2015)[10] in which ballistic tests were conducted on PMHS protected by an intergral UHMWPE helmet. Their impact velocities fell in the range of 400-460 ms^{-1} employing the same ammunition than the present work. Even though bullet perforation is not reported by Rafaels et al., severe skull fractures were obtained at impact velocities in the upper range of their sample. This fact suggests a lower head trauma prevention of the UHMWPE helmet with respect to other helmet models. For instance, Freitas et al. (2014)[9] using 9 mm FMJ bullets at velocities of about 430 ms^{-1} impacting para-aramid based helmets, reported no skull fractures.

Focusing on the aramid-alone cases, #S1, whose fabric plies are all oriented 0°/90°, is able to absorb 6% more energy than #S2, which alternates the orientations 0°/90°and 45°/-45°between adyacent plies. Nonetheless, energy should not be the only criterion to determine the protection level of a shell configuration. In fact, as can be seen in Fig. 4, the stress distribution in the frontal region of the helmet differs between #S1 and #S2 due to the fiber directions. In #S1, stresses concentrate coinciding with the sagittal plane of the head, which makes the deformation of the helmet shell higher in this direction. This fact leads to an increased value of the BFD striking the head, which in the end causes the fracture pattern depicted in Fig 6 (left). Nonetheless, no cracks are found when the head is protected with the #S2 helmet (Fig. 6 middle left). The scope of the results presented in this study is, however, limited to four cases of study. More hybrid configurations involving different ply distributions or materials should be studied to draw determining conclusions about their protective capacity when applied to combat helmets. According to our results, an aramid-fabrid setup with 16 plies of alternating orientations (case #S2) offers the best protection level between the cases studied. However, experimental validation should be performed for a deeper study, as in the manufacturing process it is difficult to ensure the proper orientation of the fabric in all the regions of the helmet shell. Aditionally, in this study we have focused in head trauma prevention against a specific ammunition type. Other parameters of the ballistic performance of the helmet may not be improved, even diminished, by the alternated orientations of the shell layers. Regarding the head model employed, more specific intracranial injuries could be predicted using a more detailed model. However, the assessment of skull fracture is sufficient to predict potential head injuries, as more complex models would involve a much greater computational cost.

Conclusions

In this work, ballistic simulations against a head wearing a combat helmet with different shell configurations have been performed with the purpose of finding an optimal construction to prevent head trauma. Two aramid and two hybrid (aramid and UHWPME) shell setups were tested, obtaining the following conclusions:

- The hybrid configurations studied do not prevent from bullet penetration. However, this perforation can be delayed by adding more aramid layers in the striking surface of the helmet, at the cost of increasing the weight of the shell.
- Aramid 16-ply configurations were able to avoid penetration of the bullet and absorb a significant extent (up to 67%) of the initial kinetic energy of the bullet.
- Following the criterion of energy absorption, the optimal configuration would be #S1, with all the aramid plies fabrics oriented at 0°/90°. However, BFD values at the frontal site are greater and this results in basilar skull fractures, which are critical to the subject.
- An aramid 16-ply setup with alternating orientations of 0°/90°and 45°/-45°between layers offers a good performance in terms of impact energy dissipation with a reasonable value of BFD. No cranial injuries were found when using this protection.

Acknowledgments

The authors gratefully acknowledge the funding support received from the Spanish Ministry of Economy and Competitiveness in the framework of the projects DPI2013-46641-R and DPI2017-89197-C2-2-R and to the Generalitat Valenciana in the context of the Programme PROMETEO 2016/007.

REFERENCES

References

1. Folio L., Solomon, J., Biassou N., Fischer T., Dworzak J., Raymont V., et al. Semi-automated trajectory analysis of deep ballistic penetrating brain injury. Mil Med 2013;178(3)338–45. https://doi.org/10.7205/MILMED-D-12-00353
2. Salman S.D., Leman Z., Sultan M.T.H., Ishak M.R., Cardona F. Ballistic impact resistance of plain woven kenaf/aramid reinforced polyvinil butyral laminated hybrid composite. BioResources 2016;11(3):7282–95. https://doi.org/10.15376/biores.11.3.7282-7295

3. Kulkarni S.G., Gao X.L., Horner S.E., Zheng J.Q., David N.V. Ballistic helmets - their design, materials and performance against traumatic brain injury. Compos Struct 2013;101:313–31. https://doi.org/10.1016/j.compstruct.2013.02.014
4. Hisley D.M., Gurganus J.C., Drysdale A.W. Experimental methodology using digital image correlation to assess ballistic helmet blunt trauma. J Appl Mech 2011;38(5).ASME. https://doi.org/10.1115/1.4004332
5. Edwards T.D., Bain E.D., Cole S.T., Freeney R.M., Halls V.A., Ivancik J., et al. Mechanical properties of silicone based composites as a temperature insensitive ballistic backing material for quantifying back face deformation. Forensic Sci Int 2018;285:1–12. https://doi.org/10.1016/j.forsciint.2018.01.014
6. Bandaru A.K., Ahmad S. Modeling progressive damage for composites under ballistic impact. Composites Part B 2016;93:75–87. http://dx.doi.org/10.1016/j.compositesb.2016.02.053
7. Martínez-Hergueta F., Ridruejo A., González C., Llorca J. Ballistic performance of hybrid nonwoven/woven polyethylene fabric shields. Int J Impact Eng 2017;111:55–65. http://dx.doi.org/10.1016/j.ijimpeng.2017.08.011
8. Sarron J.C., Dannawi M., Faure A., Caillou J.P., Da Cunha J., Robert R. Dynamic effects of a 9 mm missile on cadaveric skull protected by aramid, polyehylene or aluminum plate: an experimental study. J Trauma 2004;57(2):236–43. https://doi.org/10.1097/01.TA.0000133575.48065.3F
9. Freitas C.J., Mathis J.T., Scott N., Bigger R.P., MacKiewicz J. Dynamic response due to behind helmet blunt trauma measured with human head surrogate. Int J Med Sci 2014;11(5):409–25. https://doi.org/10.7150/ijms.8079
10. Rafaels K.A., Cutcliffe H.C., Salzar R.S., Davis M., Boggess B., Bush B., et al. Injuries of the head from backface deformation of ballistic protective helmets under ballistic impact. J Forensic Sci 2015;60(1):219–25. https://doi.org/10.1111/1556-4029.12570
11. Vargas-Gonzalez L.R., Gurganus J.C. Hybridized composite architecture for mitigation of non-penetrating ballistic trauma. Int J Impact Eng 2015; 86:295–306. http://dx.doi.org/10.1016/j.ijimpeng.2015.08.014
12. Abrate S. Modeling of impacts on composite structures. Compos Struct 2001;51(2):129–38. https://doi.org/10.1016/S0263-8223(00)00138-0
13. Yen C.F. A ballistic material model for continuous-fiber reinforced composites. Int J Impact Eng 2012;46:11–22. https://doi.org/10.1016/j.ijimpeng.2011.12.007
14. Van Hoof J., Woeswick M.J., Straznicky P.V., Bolduc M., Tylko S. Simulation of ballistic impact response of composite helmets. In: Proceedings of the 5th international LS-DYNA users conference; 1998.

15. Davies G.A.O., Zhang X. Impact damage prediction in carbon composite structures. Int J Impact Eng 1995;16:149–70. https://doi.org/10.1016/0734-743X(94)00039-Y
16. Yang Y., Chen X. Investigation on energy absorption efficiency of each layer in ballistic armour panel for applications in hybrid design. Compos Struct 2017;164:1–9. http://dx.doi.org/10.1016/j.compstruct.2016.12.057
17. Lozano-Mínguez E., Palomar M., Infante-Garía D., Rupérez M.J., Giner E. Assessment of mechanical properties of human head tissues for trauma modelling. Int J Numer Method Biomed End 2018;34(5):e2962. https://doi.org/10.1002/cnm.2962
18. Yoganandan N., Pintar F.A., Sances A., et al. Biomechanics of skull fracture. J Neurotrauma 1995;12(4):659–68. https://doi.org/10.1089/neu.1995.12.659
19. Nahum A.M., Smith R., Ward C.C. Intracranial pressure dynamics during head impact. In: SAE Technical Papers; 1977. https://doi.org/10.4271/770922
20. Palomar M., Lozano-Mínguez E., Rodríguez-Millán M., Miguélez M.H., Giner E. Relevant factors in the design of composite ballistic helmets. Compos Struct 2018;201(1):49–61. https://doi.org/10.1016/j.compstruct.2018.05.076
21. Dassault Systèmes. Abaqus 6.12 User's Manual;2012.
22. Dassault Systèmes. Section 1.2.19 VUSDFLD, Abaqus User Subroutines Reference Manual; 2012.
23. Sahoo D., Deck C., Yoganandan N., Willinger R. Development of skull fracture criterion based on real-world head trauma simulations using finite element head model. J Mech Behav Biomed Mater 2016;57:24–41. https://doi.org/10.1016/j.jmbbm.2015.11.014
24. Tan L.B., Tse K.M., Lee H.P., Tan V.B.C., Lim S.P. Performance of an advanced combat helmet with different interior cushioning systems in ballistic impact: experiments and finite element simulations. Int J Impact Eng 2012;50:99–112. https://doi.org/10.1016/j.ijimpeng.2012.06.003
25. Shen Z., Hu D., Zhang Y., Cai Q., Han X. Continuous twice-impacts analysis of UHMWPE laminate fixed with bolted joints. Int J Impact Eng 2017;109:293–301. https://doi.org/10.1016/j.ijimpeng.2017.07.013
26. Rodríguez-Millán M., Ito T., Loya J.A., Olmedo A., Miguélez. Development of numerical model for ballistic resistance evaluation of combat helmet and experimental validation. Mater Des 2016;110:391–403. https://doi.org/10.1016/j.matdes.2016.08.015
27. Lässig, T., Nguyen, L., May, M., Riedel, W., Heisserer, U., Van Der Werff, H., Hiermaier, S. A non-linear orthotropic hydrocode model for ultra-high molecular weight polyethylene in impact simulations. Int J of Impact Eng, 2015;75:110-122. https://doi.org/10.1016/j.ijimpeng.2014.07.004
28. Nguyen, L. H., Lässig, T. R., Ryan, S., Riedel, W., Mouritz, A. P., Orifici, A. C. Numerical modelling of ultra-high molecular weight polyethylene composite

under impact loading. In Procedia Engineering 2015;103:436-443. Elsevier Ltd. https://doi.org/10.1016/j.proeng.2015.04.043

29. Tham, C. Y., Tan, V. B. C., Lee, H. P. Ballistic impact of a KEVLAR® helmet: Experiment and simulations. Int J Impact Eng 2008;35(5): 304-318. https://doi.org/10.1016/j.ijimpeng.2007.03.008
30. Tse, K., Tan, L., Yang, B., Tan, V., Lim, S., Lee, H., Ballistic Impacts of a Full-Metal Jacketed (FMJ) Bullet on a Validated Finite Element (FE) Model of Helmet-Cushion-Head. The 5th International Conference on Computational Methods (ICCM), 2014.
31. Wiśniewski A., Gmitrzuk M. Validation of numerical model of the Twaron® CT709 ballistic fabric. Problems of mechatronics, armament, aviation, safety engineering 2014;16:19–32.